



Contents lists available at ScienceDirect

Journal of Quantitative Spectroscopy & Radiative Transfer

journal homepage: www.elsevier.com/locate/jqsrt



Global fittings of $^{14}\text{N}^{15}\text{N}^{16}\text{O}$ and $^{15}\text{N}^{14}\text{N}^{16}\text{O}$ vibrational–rotational line positions using the effective Hamiltonian approach

S.A. Tashkun^{a,*}, V.I. Perevalov^a, R.V. Kochanov^a, A.-W. Liu^b, S.-M. Hu^b

^a Laboratory of Theoretical Spectroscopy, Zuev Institute of Atmospheric Optics, 1 Akademicheskii av., 634021 Tomsk, Russia

^b Hefei National Laboratory for Physical Sciences at Microscale, University of Science and Technology of China, Hefei 230026, China

ARTICLE INFO

Article history:

Received 2 November 2009

Received in revised form

15 January 2010

Accepted 15 January 2010

Keywords:

Nitrous oxide isotopologues

$^{14}\text{N}^{15}\text{N}^{16}\text{O}$

$^{15}\text{N}^{14}\text{N}^{16}\text{O}$

Microwave

Infrared

Global modeling

HITRAN

ABSTRACT

An effective Hamiltonian built up to sixth order in the Amat–Nielsen ordering scheme describing all rovibrational energy levels in the ground electronic state and containing in explicit form all resonance interaction terms due to the approximate relations between harmonic frequencies $\omega_1 \approx 2\omega_2$ and $\omega_3 \approx 4\omega_2$ was applied to model the observed rovibrational line positions (collected from the literature) of $^{14}\text{N}^{15}\text{N}^{16}\text{O}$ and $^{15}\text{N}^{14}\text{N}^{16}\text{O}$ isotopologues of nitrous oxide. For $^{14}\text{N}^{15}\text{N}^{16}\text{O}$, 124 effective Hamiltonian parameters were fitted to near 28 000 observed line positions covering the 0.8–8860 cm⁻¹ spectral range. The RMS of the weighted fit is 0.00126 cm⁻¹ and dimensionless standard deviation is 1.48. For $^{15}\text{N}^{14}\text{N}^{16}\text{O}$, 121 effective Hamiltonian parameters were fitted to more than 31 000 observed line positions covering the same spectral interval. The RMS of the weighted fit is 0.00185 cm⁻¹ and dimensionless standard deviation is 1.85. In both cases the models describe all available line positions with precision compatible to the measurement uncertainties. A number of local resonance perturbations was found and discussed. Among these perturbations there are interpolyad resonance Coriolis interactions. A comparison of HITRAN-2008 data with the calculations based on the fitted models is presented.

© 2010 Elsevier Ltd. All rights reserved.

1. Introduction

This paper is the continuation of our effort for modeling high-resolution spectra of nitrous oxide (N_2O) isotopologues using the effective Hamiltonian approach [1–6]. Current study is devoted to $^{14}\text{N}^{15}\text{N}^{16}\text{O}$ and $^{15}\text{N}^{14}\text{N}^{16}\text{O}$. N_2O is a minor constituent of the earth atmosphere, but it plays an important role in physical and chemical processes. Despite relatively small natural isotopic abundance (0.0036409) $^{14}\text{N}^{15}\text{N}^{16}\text{O}$ and $^{15}\text{N}^{14}\text{N}^{16}\text{O}$ play a nonnegligible role in the radiative properties of the atmosphere. Note that these two isotopologues are in the current version of the HITRAN database [7]. The purpose of the present study is to build effective Hamiltonian models which globally

describe all known observed line positions from microwave to near infrared spectral regions with a precision close to the experimental uncertainties. The results of fittings can be useful for development of the theoretical models describing the influence of the isotopic substitution on the spectral line parameters.

The paper is organized as follows. In Section 1 the effective Hamiltonian model is presented and discussed. The observed $^{14}\text{N}^{15}\text{N}^{16}\text{O}$ rovibrational line positions collected from the literature are presented in Section 2. The results of the global fit of the parameters of the effective Hamiltonian model to these data are discussed in Section 3. Similarly, in Sections 4 and 5 the analogous treatment is performed for $^{15}\text{N}^{14}\text{N}^{16}\text{O}$. Local perturbations found in the present study are discussed in Section 7. Comparison of HITRAN-2008 line positions and positions calculated from fitted models is presented in Section 8. Finally, conclusions are given in Section 9.

* Corresponding author. Tel.: +7 382 2 49 17 94; fax: +7 382 2 49 20 86.
E-mail address: tashkun@rambler.ru (S.A. Tashkun).

2. Effective Hamiltonian

The effective Hamiltonian H^{eff} globally describing the rovibrational states of N₂O was discussed in Refs. [8,9]. H^{eff} is based on a polyad structure following from the approximate relations between the harmonic frequencies $\omega_3 \approx 2\omega_1 \approx 4\omega_2$. (1)

As a result, the vibrational states can be grouped into *polyads* with the pseudo quantum number P :

$$P = 2V_1 + V_2 + 4V_3, \quad (2)$$

where V_1 , V_2 , and V_3 are the principal vibrational quantum numbers associated to the ω_1 stretch (\sum^+), ω_2 bend (Π) and ω_3 stretch (\sum^+) modes, respectively. H^{eff} takes into account two types of accidental resonance interactions: anharmonic resonance interactions and anharmonic $+\ell$ -type resonance interactions. It should be emphasized that according to Eq. (2) all resonance Coriolis interactions with odd ΔV_2 correspond to interpolyad interactions. They connect two adjacent polyads. If one neglects all Coriolis and all anharmonic interpolyad resonance interactions, one arrives to a polyad model of H^{eff} which was used in the present work. Within this model each polyad can be diagonalized independently. Applicability of the polyad model to N₂O is discussed in Ref. [1].

H^{eff} model is characterized by its matrix elements in the basis of the eigenfunctions of harmonic oscillators $|V_1 V_2 \ell_2 V_3\rangle$ and rigid rotor $|JM K=\ell_2\rangle$ operators. Here ℓ_2 is the vibrational angular momentum quantum number, J and K are the quantum numbers of the total angular momentum and its projection on the molecular-fixed z axis. Below we give the matrix elements of the effective Hamiltonian up to 6th order of the perturbation theory in a compact form. All anharmonic resonance interactions accounted in this work are listed in Table 1.

Diagonal matrix element:

$$\langle V_1, V_2, \ell_2, V_3, J | H^{\text{eff}} | V_1, V_2, \ell_2, V_3, J \rangle = \sum_i \omega_i W_i + \sum_{ij} x_{ij} W_i W_j + x_{\ell\ell} \ell_2^2 + \sum_{ijk} y_{ijk} W_i W_j W_k + \sum_i y_{i\ell\ell} W_i \ell_2^2$$

$$\begin{aligned} \langle V_1, V_2, \ell_2, V_3, J | H^{\text{eff}} | V_1 + \Delta V_1, V_2 + \Delta V_2, \ell_2 + 2s, V_3 + \Delta V_3, J \rangle &= \sqrt{[J(J+1) - \ell_2(\ell_2+s)][J(J+1) - (\ell_2+s)(\ell_2+2s)]} \\ &\times \sqrt{(V_1 + C_1)^{[\Delta V_1, 1]} (V_2 + s\ell_2 + C_2)^{[\Delta V_2/2 + 1, 2]} (V_2 - s\ell_2 + C_2)^{[\Delta V_2/2 - 1, 2]} (V_3 + C_3)^{[\Delta V_3, 1]}} \\ &\times \left\{ F_L^{(r)} + \sum_i F_{Li}^{(r)} U_i + F_{ij}^{(r)} U_i U_j + F_{\ell\ell}^{(r)} \ell_2^2 + F_j^{(r)} [J(J+1) - \ell_2^2] \right\}, \end{aligned} \quad (6)$$

Table 1
List of anharmonic resonances.

Index r	ΔV_1	ΔV_2	ΔV_3
1	-1	2	0
2	-2	0	1
3	-1	-2	1
4	0	-4	1
5	-2	4	0
6	-4	0	2
7	-3	2	1
8	-3	-2	2
9	-2	-4	2
10	1	-6	1

$$\begin{aligned} &+ \sum_{ijkm} z_{ijkm} W_i W_j W_k W_m + \sum_{ij} z_{ij\ell\ell} W_i W_j \ell_2^2 + z_{\ell\ell\ell\ell} \ell_2^4 \\ &+ \left\{ B_e - \sum_i \alpha_i W_i + \sum_{ij} \gamma_{ij} W_i W_j + \gamma_{\ell\ell} \ell_2^2 + \sum_{ijk} \varepsilon_{ijk} W_i W_j W_k \right. \\ &\quad \left. + \sum_i \varepsilon_{i\ell\ell} W_i \ell_2^2 \right\} [J(J+1) - \ell_2^2] - \left\{ D_e + \sum_i \beta_i W_i + \sum_{ij} \eta_{ij} W_i W_j \right. \\ &\quad \left. + \eta_{\ell\ell} \ell_2^2 \right\} [J(J+1) - \ell_2^2]^2 + H_e [J(J+1) - \ell_2^2]^3. \end{aligned} \quad (3)$$

ℓ -doubling matrix element:

$$\begin{aligned} \langle V_1, V_2, \ell_2, V_3, J | H^{\text{eff}} | V_1, V_2, \ell_2 \pm 2, V_3, J \rangle &= \sqrt{(V_2 \pm \ell_2 + 2)(V_2 \mp \ell_2)[J(J+1) - \ell_2(\ell_2 \pm 1)][J(J+1) - (\ell_2 \pm 1)(\ell_2 \pm 2)]} \\ &\times \{L_e + \sum_i L_i W_i + \sum_{ij} L_{ij} W_i W_j + L_j [J(J+1) - (\ell_2 \pm 1)^2]\}, \end{aligned} \quad (4)$$

where $W_i = V_i + g_i/2$, g_i is the degeneracy of the i th vibrational mode: $g_i = 1$ for $i=1,3$ and $g_i = 2$ for $i=2$, ω_i , x_{ij} , $x_{\ell\ell}$, y_{ijk} , z_{ijkm} , $z_{j\ell\ell\ell}$, B_e , α_i , γ_{ij} , ε_{ijk} , $\varepsilon_{i\ell\ell}$, D_e , β_i , η_{ij} , H_e , L_e , L_i , L_{ij} and L_j are diagonal parameters of H^{eff} .

Matrix elements of anharmonic resonance interactions:¹

$$\begin{aligned} \langle V_1, V_2, \ell_2, V_3, J | H^{\text{eff}} | V_1 + \Delta V_1, V_2 + \Delta V_2, \ell_2, V_3 + \Delta V_3, J \rangle &= \sqrt{(V_1 + C_1)^{[\Delta V_1, 1]} (V_2 - \ell_2 + C_2)^{[\Delta V_2/2, 2]} (V_2 + \ell_2 + C_2)^{[\Delta V_2/2, 2]} (V_3 + C_3)^{[\Delta V_3, 1]}} \\ &\times \left\{ F_e^{(r)} + \sum_i F_{Li}^{(r)} U_i + \sum_{ij} F_{ij}^{(r)} U_i U_j + F_{\ell\ell}^{(r)} \ell_2^2 + F_j^{(r)} [J(J+1) - \ell_2^2] \right\}, \end{aligned} \quad (5)$$

where $U_i = V_i + \Delta V_i + g_i/2$, $C_i = g_i$ if $\Delta V_i > 0$ and zero otherwise. $V^{[m,d]}$ is a factorial polynomial defined as $V^{[0,0]} = 1$, $0^{[m,d]} = 0$, $V^{[m,d]} = V(V+d)(V+2d)\dots$ if $m > 0$ and $V^{[m,d]} = V(V-d)(V-2d)\dots$ if $m < 0$. Number of factors is equal $|m|$. The upper index r specifies the resonance which depends on ΔV_i . r runs from 1 to 10. $F_e^{(r)}$, $F_{Li}^{(r)}$, $F_{ij}^{(r)}$ and $F_j^{(r)}$ are anharmonic interaction parameters of H^{eff} .

Matrix elements of anharmonic $+\ell$ -type resonance interactions:

$$\begin{aligned} \langle V_1, V_2, \ell_2, V_3, J | H^{\text{eff}} | V_1 + s, V_2 + \Delta V_2, \ell_2, V_3 + \Delta V_3, J \rangle &= \sqrt{[J(J+1) - \ell_2(\ell_2+s)][J(J+1) - (\ell_2+s)(\ell_2+2s)]} \\ &\times \sqrt{(V_1 + C_1)^{[\Delta V_1, 1]} (V_2 + s\ell_2 + C_2)^{[\Delta V_2/2 + 1, 2]} (V_2 - s\ell_2 + C_2)^{[\Delta V_2/2 - 1, 2]} (V_3 + C_3)^{[\Delta V_3, 1]}} \\ &\times \left\{ F_L^{(r)} + \sum_i F_{Li}^{(r)} U_i + F_{ij}^{(r)} U_i U_j + F_{\ell\ell}^{(r)} \ell_2^2 + F_j^{(r)} [J(J+1) - \ell_2^2] \right\}, \end{aligned} \quad (6)$$

where $\Delta V_2 \neq 0$, $s = \pm 1$ and $F_L^{(r)}$, $F_{Li}^{(r)}$, $F_{ij}^{(r)}$ are anharmonic $+\ell$ -type interaction parameters.

The full effective Hamiltonian matrix is block diagonal with respect to the polyad number, P , the rotational quantum number, J and Wang symmetry C , $C = \{e, f\}$ [8]. Each (P, J, C) block can be diagonalized separately. The energy levels of the block are ranked with an index i , $i = 1, 2, \dots$ increasing with the energy. Thus a rovibrational energy level can be unambiguously labeled with four

¹ There is a misprint in Eq. (11) of our previous paper [3]. The correct form of the square root expression is $\sqrt{(V_1 - 2)(V_1 - 1)V_1(V_2 + 2 - \ell_2)(V_2 + 2 + \ell_2)(V_3 + 1)}$.

quantum numbers (P, J, C, i) usually called generalized assignment. The ℓ -type and anharmonic $+\ell$ -type interactions connect states with different ℓ_2 values. However, these interactions have very limited effects for small values J , so ℓ_2 can be generally considered as a good quantum number for small J values. This enables us to label levels having symmetry C and $J = \ell_2$ with so-called cluster notation (P, ℓ_2, i) [1]. Spectroscopic community, however, uses another set of quantum numbers to label rovibrational levels, namely, $(V_1, V_2, \ell_2, V_3, J, C)$ called spectroscopic assignment. This labeling is adopted in particularly for the HITRAN database [7]. Due to the strong mixing between normal modes it is impossible for some levels to give an unambiguous spectroscopic assignment [1]. That is the case of levels whose eigenvectors are strongly delocalized among many basis functions. On the other hand, it is clear that correct labeling of energy levels must provide one-to-one correspondence between generalized and spectroscopic assignments.

3. $^{14}\text{N}^{15}\text{N}^{16}\text{O}$ input datafile

The input datafile includes observed line positions collected from the literature [3,6,10–26]. The file contains 28 722 lines and covers the $0.8\text{--}8857\text{ cm}^{-1}$ spectral range. The summary of the datafile is given in Table 2. Column 1 contains references to data sources. Column 2 indicates type of measurements: MW—microwave measurements, HET—laser heterodyne measurements, FTS—Fourier transform measurements, ICLAS—intracavity laser absorption measurements, CRDS—cavity ring down measurements. The data file was increased with a number of calculated line positions taken from Toth's calculated datafile SISAM-N2O [19] and marked as CALC in the second column of Table 2. These positions were calculated from spectroscopic constants. For the sake of weighting we assumed for these data an uncertainty 0.001 cm^{-1} . The measurement uncertainties are listed in column 3. Where it was possible the individual line position uncertainties were used. For these

Table 2

Source-by-source analysis of the experimental data and statistics of the line position fit for $^{14}\text{N}^{15}\text{N}^{16}\text{O}$.

Data source	Type of measurements ^a	Accuracy ^b	Calibration factor	N_{fit}	Spectral range (cm^{-1})	$\text{RMS}_{\text{RITZ}}^{\text{b}}$	$\text{RMS}_{\text{fit}}^{\text{b}}$
Andreev et al. [11]	MW	0.009–0.035		22	12.6–18.5	0.0002	0.033
Drouin and Maiwald [13]	MW	0.075		8	28.5–54.3	0.0111	0.110
Morino et al. [12]	MW	0.02–0.10		3	20.9–22.6	0.0096	0.048
Cole and Hudges [10]	MW	0.1		1	0.8	0.0025	0.103
Hinz et al. [14]	HET	2.0–8.0		4	1257.4–1316.1	0.61	1.855
Toth [19]	FTS	0.04		29	2130.0–3461.9	0.02	0.20
Toth [18]	FTS	0.04–0.4		327	2386.8–3463.5	0.16	0.26
Toth [16,17]	FTS	0.06		265	1102.7–2216.5	0.03	0.11
Brown and Toth [15]	FTS	0.066	0.9999998	2	1307.3–1308.0	0.05	0.019
Guelachvili and Rao [22] ^c	FTS	0.09–1.2	0.999999764	254	2112.0–2739.3	0.35	0.48
Guelachvili and Rao [22] ^d	FTS	0.09–1.5	0.999999764	121	2152.7–2215.6	0.20	0.43
Guelachvili and Rao [22] ^e	FTS	0.5	0.999999760	30	1228.9–1255.5	0.13	0.18
Guelachvili and Rao [22] ^f	FTS	0.5	0.999999760	102	1257.1–1324.3	0.59	0.67
Guelachvili and Rao [22] ^g	FTS	0.5	1.00000032	45	575.4–601.5	0.18	0.26
Toth [19]	CALC	1.0		2393	529.8–5085.7	0.48	0.72
Ni et al. [3]	FTS	1.0		10770	3496.1–8857.1	0.93	1.53
Wang et al. [6]	FTS	1.0		11583	1214.1–3465.3	0.67	0.99
Herbin et al. [26]	ICLAS	1.0		141	3910.7–4021.6	0.89	1.20
Amiot [21]	FTS	2.0	0.999999983	998	3582.7–5553.1	0.85	0.87
Wang et al. [23]	FTS	2.0		64	6402.6–6462.9	2.91	3.30
Liu et al. [24,25]	CRDS	2.0		826	5906.4–6791.7	2.01	2.36
Krell and Sams [20]	FTS	3.0	1.0000004	89	2391.6–2578.2	2.66	2.68

^a MW—microwave measurements, HET—laser heterodyne measurements, FTS—Fourier transform measurements, ICLAS—intracavity laser absorption measurements, CRDS—cavity ring down measurements, CALC—calculated line positions.

^b in MHz for MW and HET measurements and in 10^{-3} cm^{-1} for others.

^c $P=0.98\text{ torr}$, $L=20\text{ m}$, $\text{res}=0.0054\text{ cm}^{-1}$.

^d $P=0.15\text{ torr}$, $L=20\text{ m}$, $\text{res}=0.0054\text{ cm}^{-1}$.

^e $P=0.77\text{ torr}$, $L=16\text{ m}$, $\text{res}=0.0054\text{ cm}^{-1}$.

^f $P=0.03\text{ torr}$, $L=56\text{ m}$, $\text{res}=0.0054\text{ cm}^{-1}$.

^g $P=1.5\text{ torr}$, $L=1\text{ m}$, $\text{res}=0.0020\text{ cm}^{-1}$.

Table 3

Summary of global line position fits.

Isotopologue	N_{data}	Range (cm^{-1})	χ_{RITZ}	$\text{RMS}_{\text{RITZ}} (\text{cm}^{-1})$	N_{par}	χ_{fit}	$\text{RMS}_{\text{fit}} (\text{cm}^{-1})$
$^{14}\text{N}^{15}\text{N}^{16}\text{O}$	27967	0.8–8857	0.91	0.00086	124	1.48	0.00126
$^{15}\text{N}^{14}\text{N}^{16}\text{O}$	31743	0.8–8895	1.11	0.00098	121	1.85	0.00185

spectra we give the range of the actual uncertainties used. If there is no information about individual uncertainties, an average uncertainty for a data source is given.

The uncertainty of the data ranges from 9 kHz for the most precise MW measurements [11] to 0.003 cm⁻¹ for the old FTS measurements [20]. The datafile was checked for the internal consistency. A number of misassigned, misprinted or improperly measured lines were detected and removed from the datafile. The check was done by fitting energy levels to the observed line positions using the fundamental Ritz principle. Details of this approach can be found in Refs. [27,28]. The following criterion for deleting a line from the datafile was applied: if the absolute value of the weighted Ritz residual

$$r_{i \leftarrow j} = \frac{v_{i \leftarrow j}^{obs} - (E_i - E_j)}{\delta_{i \leftarrow j}^{obs}} \quad (7)$$

of a line is greater than 4, then the line is deleted from the datafile. In the above equation, $v_{i \leftarrow j}^{obs}$ and $\delta_{i \leftarrow j}^{obs}$ are observed frequency and its measurement uncertainty of a transition between an upper state i and a lower state j . E_i and E_j are corresponding Ritz energies (term values). Observed positions from Guelachvili's handbook [22] were calibrated using recommended calibration factors from [29]. Other spectra were calibrated against highly accurate MW and HET measurements. For some sources statistically significant factors were found. They are listed in column 4 of Table 2. The deletion criterion has lead to the exclusion of 327 lines from the fit. It should be noted that not all lines can be checked in this way. Only transitions belonging to nonfloating spectroscopic networks can be checked (see Ref. [28] for further detail). The weighted standard deviation of the cleaned dataset was 0.91. The RMS of residuals was 0.00086 cm⁻¹. These numbers give a quantitative measure of the internal consistency of the observed data. The numbers of fitted lines for each spectrum are given in column 5. Column 6 contains spectral ranges. The RMS of the Ritz fit is presented in column 7. It is seen that the stated accuracy of each spectrum is generally confirmed by the Ritz fit of the cleaned data. In particularly, Toth's calculated datafile SISAM. N2O [19] has actual average accuracy on the level of 0.0005 cm⁻¹.

4. ¹⁴N¹⁵N¹⁶O global fit

In 2008 we have published global modeling of ¹⁴N¹⁵N¹⁶O absorption spectrum which is mostly based on FTS spectra recorded in the 3800–9000 cm⁻¹ region [3]. Very recently a large array counting near 12 000 lines of new FTS measured data covering the 1200–3500 cm⁻¹ region was published [6]. This was the principal motivation for us to perform new global fit of line positions.

First of all we checked the quality of our published fitted parameters [3] by predicting new measurements [6,10,22] which were absent from our datafile [3]. Parameters from the set 1 [3] were taken. They reproduce data from [3] with RMS=0.0014 cm⁻¹. With the new enlarged datafile these parameters give RMS=0.0023 cm⁻¹.

We consider this as evidence that the set 1 has rather good interpolation and extrapolation properties.

The parameters of the effective Hamiltonian (3)–(6) have been fitted to observed line positions using the GIP computer code [30]. The code uses generalized assignment of energy levels. The initial values of the effective Hamiltonian parameters were taken from Ref. [3]. The aim of the fitting procedure was to minimize the weighted standard deviation χ defined according to the usual formula

$$\chi = \sqrt{\frac{\sum_{i \leftarrow j=1}^N [(v_{i \leftarrow j}^{obs} - v_{i \leftarrow j}^{calc})/\delta_{i \leftarrow j}]^2}{N-n}}, \quad (8)$$

where $v_{i \leftarrow j}^{obs}$ and $\delta_{i \leftarrow j}$ were defined earlier, $v_{i \leftarrow j}^{calc}(x) = E_i(x) - E_j(x)$ is the calculated line position, E_i and E_j are the eigenvalues of H^{eff} which correspond to the upper and lower states of the transition, respectively. N is the number of the line positions in the datafile, and n is the number of the adjusted Hamiltonian parameters (or length of parameter vector x). It is well known that due to the nonlinear dependence of the eigenvalues of the effective Hamiltonian matrix on its matrix elements, the target function χ has many minima. Frequently it is possible to find several sets of parameters which reproduce the input data approximately with the same quality. As an example, two sets of parameters called set 1 and set 2 from Ref. [3] could be considered. In order to choose the best set we have to analyze the values of the fitted parameters. Their values must qualitatively agree with the perturbation theory orders. Moreover the fitting itself is a very time consuming process since one has to try many sets of parameters to obtain a good χ .

In order to exclude parameter sets which violates the perturbation theory orders we have modified GIP. We have added to it the algorithm by Bunch and coworkers [31] of minimizing χ which honor simple bound constraints on parameters of the form $x' \leq x \leq x''$, where x' and x'' are fixed vectors—lower and upper bounds, respectively. Values of bounds are chosen to satisfy perturbation theory orders. In accordance with the well-known Amat–Nielsen ordering scheme, contributions of each term of H^{eff} (3)–(6) can be classified according to the smallness parameter $\lambda \sim (B/\omega)^{1/2}$, where B is the rotational constant and ω is mean value of harmonic frequencies. For N₂O $\lambda \sim 0.01$. This scheme was used to set approximate lower and upper bound on each H^{eff} parameter. It should be emphasized that these bounds are physically meaningful only for most significant parameters like ω_i , x_{ij} , $x_{\ell\ell}$, B_e , α_i , D_e , L_e , $F_e^{(r)}$, etc. For others the bounds based on λ are only very rough estimates. The main goal of introducing of the bounds is to preserve Amat–Nielsen ordering of H^{eff} parameters during least-squares fits. If a fitted parameter goes outside its bounds the least-squares minimizer fix it a bound value and continues iterations. To avoid 100% correlations, diagonal vibrational parameter x_{ll} was fixed to the value given in Ref. [9].

In order to describe the quality of a fit we use two additional statistics: RMS of residuals and RMS of residuals for a given source. They are defined according

Table 4Fitted effective Hamiltonian parameters of $^{14}\text{N}^{15}\text{N}^{16}\text{O}$ and $^{15}\text{N}^{14}\text{N}^{16}\text{O}$.

Par	$^{14}\text{N}^{15}\text{N}^{16}\text{O}$	$^{15}\text{N}^{14}\text{N}^{16}\text{O}$	Ord	Par	$^{14}\text{N}^{15}\text{N}^{16}\text{O}$	$^{15}\text{N}^{14}\text{N}^{16}\text{O}$	Ord
<i>Diagonal vibrational parameters</i>							
ω_1	1296.8066(12) ^a	1281.72618(64)		$y_{3\ell\ell}$	-0.32(11)	-5.486(46)	10^{-2}
ω_2	582.73286(78)	592.77730(42)		z_{1111}	-17.64(32)	-30.02(38)	10^{-4}
ω_3	2232.6981(14)	2259.1710(18)		z_{1112}	-68.6(19)	-76.69(72)	10^{-4}
x_{11}	-4.5370(29)	-4.2627(47)		z_{1113}	-22.9(25)	86.8(33)	10^{-4}
x_{12}	-5.29733(89)	-5.3565(11)		z_{1122}		-25.94(84)	10^{-4}
x_{13}	-24.711(11)	-25.217(20)		z_{1123}	-20.1(56)	197.3(57)	10^{-4}
x_{22}	1.05781(26)	1.13810(31)		z_{1133}	126.6(15)		10^{-4}
x_{23}	-13.77135(68)	-14.52574(49)		z_{1222}	34.0(10)	9.78(62)	10^{-4}
x_{33}	-14.33579(97)	-14.7442(13)		z_{1223}	89.2(34)	101.7(13)	10^{-4}
$x_{\ell\ell}^b$	-0.55570732	-0.61899868		z_{1233}	-38.5(87)	141.6(83)	10^{-4}
y_{111}	-0.605(16)		10^{-2}	z_{1333}	105.90(54)	125.5(19)	10^{-4}
y_{112}	0.60(18)		10^{-2}	z_{2222}	-5.885(80)	-3.131(57)	10^{-4}
y_{113}	-18.42(11)	-20.81(11)	10^{-2}	z_{2223}		-1.28(17)	10^{-4}
y_{122}	-7.28(15)	1.534(50)	10^{-2}	z_{2233}	24.8(26)	-19.7(12)	10^{-4}
y_{123}	31.20(32)	11.47(24)	10^{-2}	z_{2333}	15.22(53)	10.52(53)	10^{-4}
y_{133}		8.44(12)	10^{-2}	z_{3333}	16.50(35)	24.38(43)	10^{-4}
y_{222}	-0.748(14)	-2.1771(74)	10^{-2}	$z_{11\ell\ell}$	-10.49(79)		10^{-4}
y_{223}	5.03(11)	10.374(44)	10^{-2}	$z_{12\ell\ell}$	-4.29(73)	-8.50(86)	10^{-4}
y_{233}	-2.302(36)	-1.212(30)	10^{-2}	$z_{13\ell\ell}$	-50.9(29)		10^{-4}
y_{333}	-1.729(31)	-1.910(41)	10^{-2}	$z_{22\ell\ell}$	2.34(11)	3.16(16)	10^{-4}
$y_{1\ell\ell}$	5.08(12)	2.286(25)	10^{-2}	$z_{33\ell\ell}$	-24.7(25)	18.5(11)	10^{-4}
$y_{2\ell\ell}$	0.874(15)	2.179(13)	10^{-2}	$z_{\ell\ell\ell\ell}$	-2.08(14)	-3.00(20)	10^{-4}
<i>Diagonal rotational and vibrational–rotational parameters</i>							
B_e	0.42107235(13)	0.40687978(21)		ε_{222}	-0.1905(64)	-0.1460(56)	10^{-6}
α_1	1.91799(12)	1.78630(14)	10^{-3}	ε_{223}	1.768(13)	2.551(20)	10^{-6}
α_2	-0.543418(92)	-0.563164(81)	10^{-3}	ε_{233}	0.403(20)	0.286(21)	10^{-6}
α_3	3.34752(18)	3.37534(28)	10^{-3}	ε_{333}	0.112(15)	0.315(27)	10^{-6}
γ_{11}	-0.9816(45)	-0.699(22)	10^{-5}	$\varepsilon_{1\ell\ell}$		0.630(27)	10^{-6}
γ_{12}		-1.178(15)	10^{-5}	$\varepsilon_{2\ell\ell}$		0.071(16)	10^{-6}
γ_{13}	-0.496(10)	-0.952(85)	10^{-5}	$\varepsilon_{3\ell\ell}$		-1.465(17)	10^{-6}
γ_{22}	-1.1452(31)	-0.7937(41)	10^{-5}	D_e	0.173216(23)	0.160777(14)	10^{-6}
γ_{23}	2.8716(67)	2.7994(78)	10^{-5}	β_1	1.759(13)	1.371(20)	10^{-9}
γ_{33}	-0.540(11)	-0.447(18)	10^{-5}	β_2	2.497(15)	2.420(12)	10^{-9}
$\gamma_{\ell\ell}$	0.6739(38)	0.2906(49)	10^{-5}	β_3	-0.784(16)	-0.601(24)	10^{-9}
ε_{111}	-0.1750(57)	-0.1176(96)	10^{-6}	η_{11}	-8.89(45)	-8.17(71)	10^{-11}
ε_{113}	-2.996(28)	-3.963(65)	10^{-6}	η_{12}	34.6(10)		10^{-11}
ε_{122}	-0.268(42)	-0.944(39)	10^{-6}	η_{13}	1.60(75)	-11.2(13)	10^{-11}
ε_{123}	0.829(83)	-0.668(91)	10^{-6}	η_{22}	-13.24(33)	-4.45(21)	10^{-11}
ε_{133}	1.048(43)	1.577(68)	10^{-6}	η_{23}	13.15(50)	13.12(67)	10^{-11}

Table 4. (continued)

<i>Parameters of ℓ-doubling matrix element</i>				η_{33}	−7.39(75)	−7.11(99)	10^{-11}
L_e	−0.201410(22)	−0.184535(22)	10^{-3}	L_{13}	9.8(16)	−100.0 ^c	10^{-8}
L_2	−1.584(13)	−1.423(12)	10^{-6}	L_{22}	−13.39(23)	−3.89(14)	10^{-8}
L_3	3.246(19)	2.613(27)	10^{-6}	L_{23}	56.25(51)	92.7(20)	10^{-8}
L_{11}	−21.7(24)		10^{-8}	L_{33}	−17.88(54)	−13.91(77)	10^{-8}
L_{12}	48.4(17)	−29.2(12)	10^{-8}	L_j	2.538(39)	2.157(40)	10^{-10}
<i>Parameters of anharmonic-interaction matrix elements</i>							
$F_e^{(1)}$	19.02761(61)	19.69605(45)		$F_{12}^{(1)}$	−0.664(13)		10^{-2}
$F_1^{(1)}$	−0.3008(19)	−0.29605(54)		$F_{13}^{(1)}$	−2.002(56)	−2.875(32)	10^{-2}
$F_2^{(1)}$	−0.27215(48)	−0.32049(14)		$F_{33}^{(1)}$	1.232(96)		10^{-2}
$F_3^{(1)}$	−0.1762(42)			$F_{\ell\ell}^{(1)}$	−0.1688(45)	0.2025(27)	10^{-2}
$F_{11}^{(1)}$	0.282(16)		10^{-2}	$F_j^{(1)}$	−0.130024(99)	−0.119197(79)	10^{-3}
$F_e^{(2)}$	−7.620(69)	−12.197(57)		$F_{13}^{(2)}$		−3.146(55)	10^{-2}
$F_1^{(2)}$		−0.3854(15)		$F_{22}^{(2)}$	−3.04(13)	−0.402(69)	10^{-2}
$F_2^{(2)}$	0.261(12)			$F_{23}^{(2)}$	3.89(31)	4.0 ^c	10^{-2}
$F_{11}^{(2)}$	−2.397(59)		10^{-2}	$F_j^{(2)}$		−2.05(26)	10^{-5}
$F_3^{(3)}$	−1.636(30)	−1.901(12)		$F_{13}^{(3)}$		4.0 ^c	10^{-2}
$F_1^{(3)}$	−0.1712(44)	−0.2891(30)		$F_{22}^{(3)}$	0.1022(72)	0.8917(70)	10^{-2}
$F_2^{(3)}$		−0.1809(15)		$F_{23}^{(3)}$	1.226(74)	1.050(40)	10^{-2}
$F_3^{(3)}$	0.750(81)	1.220(32)	10^{-1}	$F_{33}^{(3)}$	2.789(96)		10^{-2}
$F_{11}^{(3)}$	−0.952(48)		10^{-2}	$F_{\ell\ell}^{(3)}$	0.808(27)	−0.137(16)	10^{-2}
$F_{12}^{(3)}$	1.652(54)		10^{-2}	$F_j^{(3)}$	0.4246(73)		10^{-4}
$F_e^{(4)}$	−0.2272(36)	−0.1866(16)		$F_2^{(4)}$	0.196(19)		10^{-2}
$F_1^{(4)}$	−0.780(52)	−0.665(37)	10^{-2}	$F_3^{(4)}$	4.67(10)	1.859(54)	10^{-2}
$F_e^{(5)}$	0.03336(58)	−0.00237(15)		$F_2^{(5)}$	−0.2204(43)	−0.0328(15)	10^{-2}
$F_1^{(5)}$	−0.1051(33)	−0.1055(17)	10^{-2}	$F_j^{(5)}$	−0.1634(75)	0.3066(87)	10^{-6}
$F_e^{(6)}$	0.1643(36)	0.6372(38)		$F_3^{(6)}$		−1.0 ^c	10^{-1}
$F_2^{(6)}$	6.43(26)		10^{-2}	$F_j^{(6)}$	5.89(33)	−7.53(32)	10^{-6}
$F_e^{(7)}$		0.0263(24)		$F_3^{(7)}$	0.635(73)	−1.634(72)	10^{-2}
$F_1^{(7)}$	0.824(28)	0.466(17)	10^{-2}	$F_j^{(7)}$	−4.479(95)	−1.967(56)	10^{-6}
$F_2^{(7)}$	−0.276(24)	1.147(19)	10^{-2}	$F_e^{(8)}$	−0.734(63)	0.978(17)	10^{-1}
$F_e^{(9)}$		−1.492(57)	10^{-2}	$F_e^{(10)}$	0.2122(72)	−0.0618(31)	10^{-2}
<i>Parameters of anharmonic+ℓ-type matrix elements</i>							
$F_L^{(1)}$	0.8722(19)	0.9635(19)	10^{-5}	$F_{L2}^{(1)}$	−0.1888(54)	−0.2119(49)	10^{-6}
$F_{L1}^{(1)}$	0.132(19)	0.337(12)	10^{-6}	$F_{L3}^{(1)}$		0.890(37)	10^{-6}

^a Uncertainties in parentheses represent one standard deviation in units of the last quoted digit.^b Fixed to the value given in Ref. [9].^c Parameter is constrained to its upper or lower bound.

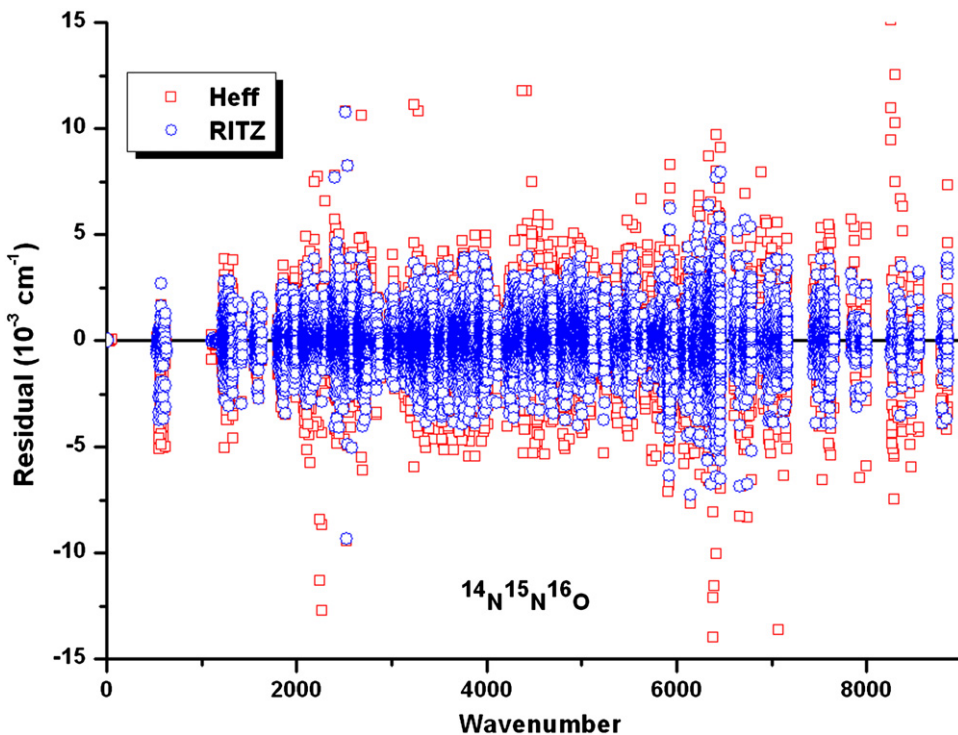


Fig. 1. $^{14}\text{N}^{15}\text{N}^{16}\text{O}$ RITZ and global fit residuals plotted versus wavenumber.

to the equation

$$RMS = \sqrt{\frac{\sum_{i-j=1}^N (v_{i-j}^{obs} - v_{i-j}^{calc})^2}{N}} \quad (9)$$

where N is the number of the fitted line positions in the first case and the number of the line positions of a source in the second case. With 124 adjustable parameters of H^{eff} within a hypercube $[x^l - x^u]$ defined by parameter bounds a local minimum was found which reproduces 27 967 observed line positions with $RMS = 0.00126\text{ cm}^{-1}$ and dimensionless standard deviation $\chi_{fit} = 1.48$. Since the algorithm [31] always finds a local minimum, the question whether the minimum found is the global one remains open. In order to reach this quality of modeling, we have removed from the datafile a number of additional lines which cannot be described by our model. These lines fall into two parts. The first part consists of the lines which cannot be checked with the RITZ code and have large residuals. These lines are either badly measured or assigned. The second part consists of the lines which were checked with the RITZ code and have large residuals despite that they are properly measured and assigned. These lines belong to bands locally perturbed by interpolyad resonance interactions which are not included in our H^{eff} models. The local perturbations will be discussed in Section 7.

The total number of removed lines was 428 and the total number of fitted vibrational states was 141. The spectrum-by-spectrum RMS of the fit is given in the last

column of Table 2. One can see that a typical ratio RMS_{fit}/RMS_{RITZ} is about two. This means that the fitted model in average reproduces line positions with accuracy compatible with measurement uncertainties. The summary of the fit are also presented in Table 3. The values of fitted parameters together with uncertainties (both in cm^{-1}) are given in the left panel of Table 4. Uncertainties in parentheses represent one standard deviation in units of the last quoted digit.

Unweighted H^{eff} and RITZ residuals are plotted in Fig. 1 versus wavenumber. H^{eff} residuals are shown in red squares and those of RITZ are shown in blue circles. The difference of spreads of red squares and blue circles gives an idea about quality of modeling. The performed modeling is close to the quality of the observed data. Vibrational levels presented in the observed datafile are listed in Table 5. The energies E of the vibrational levels and Wang symmetry are given in the first column of this table. Taking into account the RMS of the fit we believe that the accuracy of the vibrational energies is about 0.002 cm^{-1} . It should be emphasized that our E values differ from the vibrational term values G_v for the levels with $\ell_2 > 0$. In the standard expression for the rovibrational energy levels of a given vibrational state (V_1, V_2, ℓ_2, V_3, C) in the terms of the spectroscopic parameters G_v, B_v, D_v, H_v

$$F_v(J) = G_v + B_v J(J+1) - D_v J^2(J+1)^2 + H_v J^3(J+1)^3$$

the vibrational term value G_v can be formally considered as vibrational energy of the level with $J=0$, meanwhile for

Table 5Assignment and fractions respective to the basis states for the observed vibrational states of $^{14}\text{N}^{15}\text{N}^{16}\text{O}$.

E (cm $^{-1}$)	GA ^a	SA ^b	F ^c	SA ^b	F ^c	SA ^b	F ^c
576.2721e	(1,1,1)	0110e	1.00				
576.2737f	(1,1,1)	0110f	1.00				
1144.3337e	(2,0,1)	0200e	0.92	1000e	0.08		
1153.5506e	(2,2,2)	0220e	1.00				
1153.5506f	(2,2,1)	0220f	1.00				
1280.3541e	(2,0,2)	1000e	0.92	0200e	0.08		
1714.8631e	(3,1,1)	0310e	0.86	1110e	0.14		
1714.8662f	(3,1,1)	0310f	0.86	1110f	0.14		
1731.8179f	(3,3,2)	0330f	1.00				
1731.8179e	(3,3,2)	0330e	1.00				
1861.0263e	(3,1,2)	1110e	0.86	0310e	0.14		
1861.0281f	(3,1,2)	1110f	0.86	0310f	0.14		
2177.6568e	(4,0,1)	0001e	1.00				
2278.1929e	(4,0,2)	0400e	0.76	1200e	0.23		
2286.8792e	(4,2,3)	0420e	0.81	1220e	0.19		
2431.3226e	(4,0,3)	1200e	0.61	0400e	0.23	2000e	0.16
2442.1084e	(4,2,5)	1220e	0.81	0420e	0.19		
2442.1084f	(4,2,2)	1220f	0.81	0420f	0.19		
2552.4082e	(4,0,4)	2000e	0.83	1200e	0.15	0400e	0.01
2740.4301e	(5,1,1)	0111e	1.00				
2740.4317f	(5,1,1)	0111f	1.00				
2844.1917e	(5,1,2)	0510e	0.67	1310e	0.31	2110e	0.02
2844.1963f	(5,1,2)	0510f	0.67	1310f	0.31	2110f	0.02
3004.1531e	(5,1,3)	1310e	0.44	0510e	0.30	2110e	0.26
3004.1565f	(5,1,3)	1310f	0.44	0510f	0.30	2110f	0.26
3023.6755f	(5,3,5)	1330f	0.77	0530f	0.23		
3023.6755e	(5,3,5)	1330e	0.77	0530e	0.23		
3137.8095e	(5,1,4)	2110e	0.72	1310e	0.25	0510e	0.03
3137.8115f	(5,1,4)	2110f	0.72	1310f	0.25	0510f	0.03
3304.3013f	(6,2,1)	0221f	1.00				
3411.8815f	(6,2,2)	0620f	0.6	1420f	0.36	2220f	0.04
3411.8815e	(6,2,4)	0620e	0.6	1420e	0.36	2220e	0.04
3432.1931e	(6,0,3)	1001e	0.92	0201e	0.07		
3568.5186e	(6,0,4)	2200e	0.37	0600e	0.36	1400e	0.24
3709.8144e	(6,0,5)	2200e	0.34	1400e	0.34	3000e	0.24
3722.8050f	(6,2,4)	2220f	0.63	1420f	0.32	0620f	0.05
3722.8050e	(6,2,9)	2220e	0.63	1420e	0.32	0620e	0.05
3816.4769e	(6,0,6)	3000e	0.72	2200e	0.23	1400e	0.05
3852.9972e	(7,1,1)	0311e	0.87	1111e	0.13		
3853.0003f	(7,1,1)	0311f	0.87	1111f	0.13		
3999.4005e	(7,1,3)	1111e	0.86	0311e	0.13		
3999.4022f	(7,1,3)	1111f	0.86	0311f	0.13		
4135.6644e	(7,1,4)	2310e	0.42	0710e	0.40	1510e	0.12
4135.6693f	(7,1,4)	2310f	0.42	0710f	0.40	1510f	0.12
4153.7427e	(7,3,7)	0730e	0.38	2330e	0.38	1530e	0.24
4153.7427f	(7,3,7)	0730f	0.38	2330f	0.38	1530f	0.24
4284.7900e	(7,1,5)	1510e	0.37	3110e	0.36	2310e	0.16
4284.7936f	(7,1,5)	1510f	0.37	3110f	0.36	2310f	0.16
4326.6175e	(8,0,1)	0002e	1.00				
4403.7285e	(8,0,2)	0401e	0.76	1201e	0.23		
4406.9569e	(7,1,6)	3110e	0.57	2310e	0.33	1510e	0.09
4406.9592f	(7,1,6)	3110f	0.57	2310f	0.33	1510f	0.09
4412.0742e	(8,2,3)	0421e	0.82	1221e	0.18		
4556.7656e	(8,0,4)	1201e	0.62	0401e	0.22	2001e	0.15
4567.1447f	(8,2,3)	1221f	0.82	0421f	0.18		
4567.1448e	(8,2,7)	1221e	0.82	0421e	0.18		
4677.7974e	(8,0,5)	2001e	0.83	1201e	0.15	0401e	0.01
4695.2741e	(8,0,6)	0800e	0.41	2400e	0.41	3200e	0.15
4849.7624e	(8,0,7)	3200e	0.42	1600e	0.33	0800e	0.16
4861.0861f	(8,2,5)	3220f	0.42	1620f	0.36	0820f	0.15
4861.0861e	(8,2,12)	3220e	0.42	1620e	0.36	0820e	0.15
4875.8915e	(9,1,1)	0112e	1.00				
4875.8931f	(9,1,1)	0112f	1.00				
4957.1531e	(9,1,2)	0511e	0.68	1311e	0.30	2111e	0.02
4957.1576f	(9,1,2)	0511f	0.68	1311f	0.30	2111f	0.02
4979.7019e	(8,0,8)	4000e	0.33	2400e	0.33	1600e	0.17
4995.9106f	(8,2,6)	3220f	0.46	2420f	0.38	1620f	0.14
4995.9106e	(8,2,14)	3220e	0.46	2420e	0.38	1620e	0.14
5073.0681e	(8,0,9)	4000e	0.59	3200e	0.28	2400e	0.10

Table 5 (continued)

<i>E</i> (cm ⁻¹)	GA ^a	SA ^b	F ^c	SA ^b	F ^c	SA ^b	F ^c
5116.6877e	(9,1,4)	1311e	0.46	0511e	0.29	2111e	0.25
5116.6910f	(9,1,4)	1311f	0.46	0511f	0.29	2111f	0.25
5249.7732e	(9,1,5)	2111e	0.72	1311e	0.24	0511e	0.03
5249.7751f	(9,1,5)	2111f	0.72	1311f	0.24	0511f	0.03
5417.8035e	(9,1,7)	3310e	0.38	1710e	0.28	0910e	0.21
5417.8087f	(9,1,7)	3310f	0.38	1710f	0.28	0910f	0.21
5417.8910e	(10,0,1)	0202e	0.93	1002e	0.07		
5426.3566e	(10,2,2)	0222e	1.00				
5555.6439e	(10,0,3)	1002e	0.92	0202e	0.07		
5556.6935e	(9,1,8)	4110e	0.43	2510e	0.28	1710e	0.22
5556.6974f	(9,1,8)	4110f	0.43	2510f	0.28	1710f	0.22
5668.5530e	(10,0,5)	2201e	0.37	0601e	0.35	1401e	0.25
5668.9029e	(9,1,9)	4110e	0.42	3310e	0.36	2510e	0.17
5668.9056f	(9,1,9)	4110f	0.42	3310f	0.36	2510f	0.17
5678.0495f	(10,2,4)	1421f	0.34	0621f	0.34	2221f	0.32
5678.0495e	(10,2,9)	1421e	0.34	0621e	0.34	2221e	0.32
5808.9282e	(10,0,6)	2201e	0.35	1401e	0.33	3001e	0.24
5821.4700f	(10,2,5)	2221f	0.58	1421f	0.29	0621f	0.05
5821.4700e	(10,2,12)	2221e	0.58	1421e	0.29	0621e	0.05
5914.7103e	(10,0,8)	3001e	0.72	2201e	0.22	1401e	0.04
5962.4339e	(11,1,1)	0312e	0.87	1112e	0.13		
5962.4369f	(11,1,1)	0312f	0.87	1112f	0.13		
5977.2430e	(10,0,9)	3400e	0.25	0a00e	0.25	4200e	0.24
5977.9970e	(11,3,2)	0332e	1.00				
5977.9970f	(11,3,2)	0332f	1.00				
6109.4550e	(11,1,3)	1112e	0.87	0312e	0.13		
6109.4567f	(11,1,3)	1112f	0.87	0312f	0.13		
6121.7223e	(10,0,10)	4200e	0.37	1800e	0.25	2600e	0.16
6135.0077f	(10,2,8)	4220f	0.45	1820f	0.26	2620f	0.22
6135.0077e	(10,2,18)	4220e	0.45	1820e	0.26	2620e	0.22
6240.6640e	(10,0,11)	5000e	0.42	3400e	0.23	2600e	0.22
6261.7168e	(10,2,20)	3420e	0.38	4220e	0.32	2620e	0.22
6322.9960e	(10,0,12)	5000e	0.44	4200e	0.31	3400e	0.16
6370.9498e	(11,1,6)	1511e	0.32	3111e	0.30	2311e	0.14
6370.9539f	(11,1,6)	1511f	0.32	3111f	0.30	2311f	0.14
6446.8922e	(12,0,1)	0003e	1.00				
6491.8312e	(11,1,8)	3111e	0.56	2311e	0.32	1511e	0.09
6491.8334f	(11,1,8)	3111f	0.56	2311f	0.32	1511f	0.09
6653.9448e	(12,0,4)	1202e	0.63	0402e	0.22	2002e	0.15
6663.9289e	(12,2,7)	1222e	0.82	0422e	0.18		
6690.4074e	(11,1,10)	1910e	0.26	4310e	0.25	5110e	0.21
6690.4129f	(11,1,10)	1910f	0.26	4310f	0.25	5110f	0.21
6775.2219e	(12,0,7)	2002e	0.83	1202e	0.14	0402e	0.01
6819.7224e	(11,1,11)	5110e	0.45	2710e	0.24	1910e	0.13
6819.7266f	(11,1,11)	5110f	0.45	2710f	0.24	1910f	0.13
6923.1456e	(12,0,8)	3201e	0.19	1601e	0.17	0c00e	0.15
6924.1655e	(11,1,12)	4310e	0.34	5110e	0.28	3510e	0.24
6924.1688f	(11,1,12)	4310f	0.34	5110f	0.28	3510f	0.24
6982.6738e	(13,1,1)	0113e	1.00				
6982.6754f	(13,1,1)	0113f	1.00				
7051.7755e	(12,0,10)	2401e	0.33	4001e	0.33	1601e	0.16
7067.6465e	(12,2,18)	3221e	0.46	2421e	0.37	1621e	0.13
7143.3957e	(12,0,12)	4001e	0.58	3201e	0.28	2401e	0.09
7333.9332e	(13,1,7)	2112e	0.72	1312e	0.24	0512e	0.03
7333.9350f	(13,1,7)	2112f	0.72	1312f	0.24	0512f	0.03
7492.1231e	(12,0,15)	6000e	0.48	3600e	0.19	2800e	0.15
7511.6371e	(14,0,1)	0203e	0.93	1003e	0.07		
7519.7373e	(14,2,2)	0223e	1.00				
7567.4293e	(12,0,16)	5200e	0.29	6000e	0.27	4400e	0.23
7615.9825e	(13,1,10)	4111e	0.42	2511e	0.28	1711e	0.21
7615.9863f	(13,1,10)	4111f	0.42	2511f	0.28	1711f	0.21
7650.7538e	(14,0,3)	1003e	0.92	0203e	0.07		
7725.9820e	(13,1,12)	4111e	0.41	3311e	0.35	2511e	0.16
7725.9846f	(13,1,12)	4111f	0.41	3311f	0.35	2511f	0.16
7880.3875e	(14,0,8)	2202e	0.36	1402e	0.33	3002e	0.23
7985.5480e	(14,0,9)	3002e	0.71	2202e	0.22	1402e	0.04
8191.2479e	(15,1,3)	1113e	0.87	0313e	0.12		
8191.2495f	(15,1,3)	1113f	0.87	0313f	0.12		
8284.8091e	(14,0,14)	5001e	0.41	3401e	0.22	2601e	0.22
8364.6944e	(14,0,15)	5001e	0.39	4201e	0.28	3401e	0.16

Table 5 (continued)

E (cm $^{-1}$)	GA ^a	SA ^b	F ^c	SA ^b	F ^c	SA ^b	F ^c
8538.5127e	(16,0,1)	0004e	1.00				
8844.7190e	(16,0,7)	2003e	0.83	1203e	0.14	4002e	0.02

^a GA is the generalized (cluster) assignment (P, ℓ_2, i).^b SA is the spectroscopic (HITRAN) assignment V_1, V_2, ℓ_2, V_3, C . Characters a,b,c in the V_2 field corresponds to $V_2=10$, $V_2=11$, and $V_2=12$.^c Squares of the expansion coefficients of the vibrational state for the dominant basis states appearing in the preceding column.

Table 6

Source-by-source analysis of the experimental data and statistics of the line position fit for $^{15}\text{N}^{14}\text{N}^{16}\text{O}$.

Data source	Type of measurements ^a	Accuracy ^b	Calibration factor	N_{fit}	Spectral range (cm $^{-1}$)	RMS _{RITZ} ^b	RMS _{fit} ^b
Andreev et al. [11]	MW	0.009–0.035		22	13.0–18.7	0.0001	0.067
Drouin and Maiwald [13]	MW	0.075		7	29.9–54.1	0.005	0.3
Morino et al. [12]	MW	0.02–0.10		3	21.0–22.7	0.0023	0.027
Cole and Hudges [10]	MW	0.1		1	0.8	0.0025	0.015
Hinz et al. [14]	HET	2.0–8.0		3	1257.4–1295.5	1.49	2.58
Toth [19]	FTS	0.04		81	2143.6–3465.7	0.02	0.11
Toth [18]	FTS	0.04–0.4		321	2391.5–3474.4	0.15	0.27
Toth [16,17]	FTS	0.06		264	1115.4–2240.4	0.03	0.13
Guelachvili and Rao [22] ^c	FTS	0.09–1.2	0.999999764	197	1862.1–2772.4	0.48	0.57
Guelachvili and Rao [22] ^d	FTS	0.09–1.5	0.999999764	168	2153.0–2220.9	0.29	0.47
Guelachvili and Rao [22] ^e	FTS	0.5	0.999999760	69	1134.9–1250.5	0.90	0.99
Guelachvili and Rao [22] ^f	FTS	0.5	0.999999760	92	1250.9–1312.0	0.58	0.72
Guelachvili and Rao [22] ^g	FTS	0.5	1.00000032	45	585.3–605.7	0.24	0.22
Toth [19]	CALC	1.0		1630	540.6–4703.0	0.67	0.96
Ni et al. [32]	FTS	1.0		632	1842.0–8640.4	0.82	2.09
Song et al. [4]	FTS	1.0		13964	3475.0–8894.5	1.18	2.41
Wang et al. [6]	FTS	1.0		12646	1214.3–3626.6	0.67	1.09
Herbin et al. [26]	ICLAS	1.0		129	3953.1–4033.3	0.92	1.36
Amiot [21]	FTS	2.0	0.999999983	647	3582.6–5080.9	1.20	1.31
Liu et al. [24,25]	CRDS	2.0		780	5906.0–6812.1	1.95	2.86

^a MW—microwave measurements, HET—laser heterodyne measurements, FTS—Fourier transform measurements, ICLAS—intracavity laser absorption measurements, CRDS—cavity ring down measurements, CALC—calculated line positions.^b in MHz for MW and HET measurements and in 10 $^{-3}$ cm $^{-1}$ for others.^c $P=0.98$ torr, $L=20$ m, res=0.0054 cm $^{-1}$.^d $P=0.15$ torr, $L=20$ m, res=0.0054 cm $^{-1}$.^e $P=0.77$ torr, $L=16$ m, res=0.0054 cm $^{-1}$.^f $P=0.03$ torr, $L=56$ m, res=0.0054 cm $^{-1}$.^g $P=1.5$ torr, $L=1$ m, res=0.0020 cm $^{-1}$.

all existing levels the inequality $J \geq \ell_2$ always has to be satisfied. Unambiguous cluster notations in the form (P, ℓ_2, i) are given in column 2 of this table. The columns 3 and 4 contain dominant basis function and square of the expansion coefficient (fraction) which stands before this function. The second and the third dominant pairs (if any) are listed in columns 5–8. The lower limit for outputting fractions is set to 0.01. It is seen that there are a number of levels having the same leading dominant basis function. For these levels it is impossible to give unambiguous spectroscopic assignment. This assignment for them is a matter of convention. For example the eigenstate with the cluster assignment (6, 0, 4) corresponding to the vibrational level value 3568.5186 cm $^{-1}$ is strongly delocalized. According to the dominant contribution it should be assigned to 2200e. Amiot [21] has assigned this level to 1400e. The question who is wrong is meaningless since V_1 and V_2 are bad (approximate) quantum numbers.

5. $^{15}\text{N}^{14}\text{N}^{16}\text{O}$ input datafile

The input datafile includes observed line positions collected from the literature [4,6,10–14,16–19,21,22,24–26,32]. The file has 33 057 lines and covers the 0.8–8895 cm $^{-1}$ spectral range. The overwhelming majority of observed data came from Refs. [4,6] covering the 1214–8895 cm $^{-1}$ spectral range. The summary of the datafile is given in Table 6. This table has the same structure as Table 2. Application of the criterion of Eq. (7) has lead to the exclusion from the fit 732 lines which were considered as misassigned, misprinted or improperly measured. The weighted standard deviation of the cleaned dataset is 1.11. The RMS of residuals is 0.00098 cm $^{-1}$. These numbers give a quantitative measure of the internal consistency of the observed data. The RMS of the Ritz fit is presented in column 7 of this table. As in the case of $^{14}\text{N}^{15}\text{N}^{16}\text{O}$ it is seen that the stated accuracy of each spectrum is generally confirmed

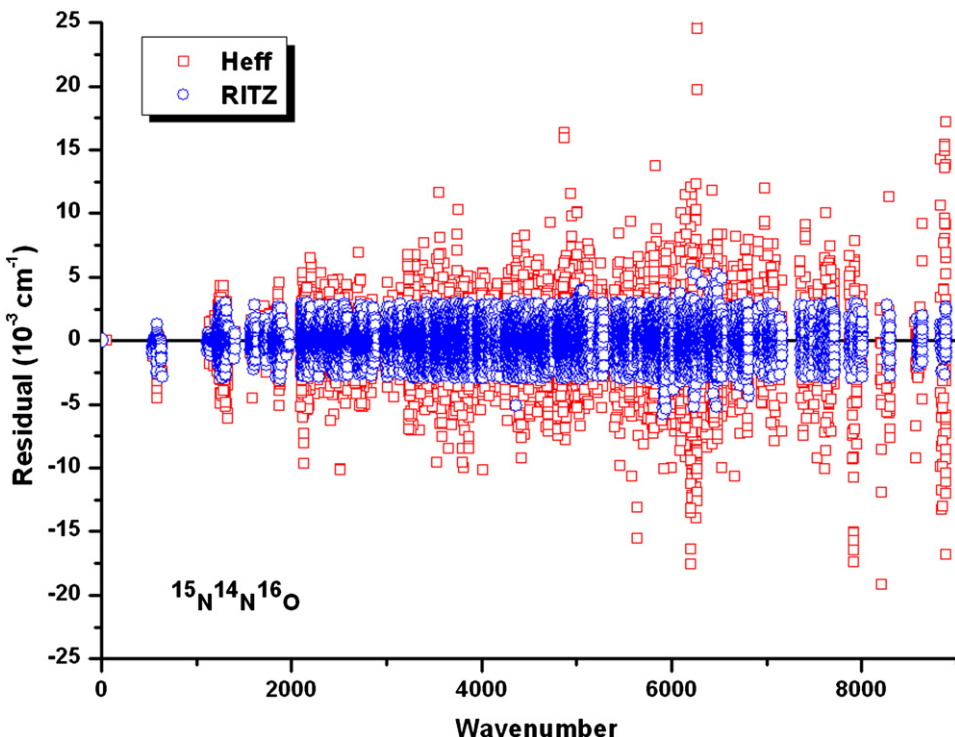


Fig. 2. $^{15}\text{N}^{14}\text{N}^{16}\text{O}$ RITZ and global fit residuals plotted versus wavenumber.

by the Ritz fit of the cleaned data. Before the present work the most extensive study of this isotopologue was done by Amiot [21]. Using a FT spectrometer he has measured and analyzed 69 bands from 1750 to 6000 cm^{-1} . In particular he found a number of local resonances in the vibrational states 1001e, 0601e, 1111f and 1201e.

6. $^{15}\text{N}^{14}\text{N}^{16}\text{O}$ global fit

As in the case of $^{14}\text{N}^{15}\text{N}^{16}\text{O}$, parameters of the effective Hamiltonian (see Eqs. (3–6)) were fitted to the cleaned datafile. The adjustable parameters were constrained using the same upper and lower bounds as for $^{14}\text{N}^{15}\text{N}^{16}\text{O}$. With 121 adjustable parameters we were able to reproduce the positions of 31 699 rovibrational lines belonging to more than 400 bands with RMS=0.00185 cm^{-1} and dimensionless standard deviation $\chi_{\text{fit}}=1.85$. To reach these results we have removed from the datafile 582 lines. Among them there are lines which are badly measured, badly assigned or perturbed by interpolyad resonance Coriolis interactions. The fit summary is presented in Table 3. It turned out that the values of four adjustable parameters namely L_{13} , $F_{23}^{(2)}$, $F_{13}^{(3)}$ and $F_3^{(6)}$ went outside prescribed upper or lower bounds during the fit. They were constrained to their bound values. The quality of the fit for this isotopologue is slightly worse than for $^{14}\text{N}^{15}\text{N}^{16}\text{O}$. The reason is that the number of fitted data as well as the number of fitted vibrational states is larger in the case of $^{15}\text{N}^{14}\text{N}^{16}\text{O}$ and the number of interpolyad resonance Coriolis interactions which are not taken into account by our polyad model of H^{eff} is also larger in this

case than for $^{14}\text{N}^{15}\text{N}^{16}\text{O}$. The values of fitted parameters together with uncertainties (both in cm^{-1}) are given in Table 4. Unweighted H^{eff} and RITZ residuals are plotted in Fig. 2 versus a wavenumber using the same symbols as in Fig. 1. The spreads of red squares and blue circles in this case are larger than for $^{14}\text{N}^{15}\text{N}^{16}\text{O}$. The vibrational levels included into observed datafile are listed in Table 5.

7. Local perturbations

In the case of $^{14}\text{N}^{15}\text{N}^{16}\text{O}$ Amiot [21] observed a local resonance perturbations for the 3110e–0110e and 0401e–0200e bands around $J=25$. We confirmed his result in Ref. [3] attributing this perturbation to an interpolyad resonance Coriolis interaction. Besides, several other perturbations were found and reported in Ref. [3]. Global fit presented in the current study does not reveal any additional perturbations.

In the case of $^{15}\text{N}^{14}\text{N}^{16}\text{O}$ Amiot [21] has found that four levels 1001e, 0600e, 1201e and 1111f are perturbed by resonance Coriolis interactions. He assigned energy levels located at 3443.652 cm^{-1} and 3439.374 cm^{-1} to 1001e and 0600e vibrational states, respectively. According to our analysis given in Table 7 the state at 3443.652 cm^{-1} is well localized at low J values and also assigned to 1001e. Another state at 3439.374 cm^{-1} is a delocalized one. It can equally be assigned either to 1400e or to 0600e. Both states are involved into the sequence of the resonance anharmonic interactions ($r=1–5, 7, 10$ according to notations given in Table 1).

Table 7Assignment and fractions respective to the basis states for the observed vibrational states of $^{15}\text{N}^{14}\text{N}^{16}\text{O}$.

E (cm $^{-1}$)	GA ^a	SA ^b	F ^c	SA ^b	F ^c	SA ^b	F ^c
586.1221e	(1,1,1)	0110e	1.00				
586.1236f	(1,1,1)	0110f	1.00				
1159.9719e	(2,0,1)	0200e	0.86	1000e	0.13		
1173.2796f	(2,2,1)	0220f	1.00				
1173.2796e	(2,2,2)	0220e	1.00				
1269.8921e	(2,0,2)	1000e	0.86	0200e	0.13		
1737.4580e	(3,1,1)	0310e	0.78	1110e	0.22		
1737.4607f	(3,1,1)	0310f	0.78	1110f	0.22		
1761.4558f	(3,3,2)	0330f	1.00				
1761.4558e	(3,3,2)	0330e	1.00				
1863.5738e	(3,1,2)	1110e	0.78	0310e	0.22		
1863.5755f	(3,1,2)	1110f	0.78	0310f	0.22		
2201.6053e	(4,0,1)	0001e	1.00				
2305.1624e	(4,0,2)	0400e	0.64	1200e	0.33	2000e	0.02
2317.1165e	(4,2,3)	0420e	0.72	1220e	0.28		
2350.6302e	(4,4,4)	0440e	1.00				
2439.6245e	(4,0,3)	1200e	0.40	0400e	0.31	2000e	0.28
2457.0333f	(4,2,2)	1220f	0.72	0420f	0.28		
2457.0333e	(4,2,5)	1220e	0.72	0420e	0.28		
2534.5319e	(4,0,4)	2000e	0.69	1200e	0.26	0400e	0.04
2773.5064e	(5,1,1)	0111e	1.00				
2773.5079f	(5,1,1)	0111f	1.00				
2876.5831e	(5,1,2)	0510e	0.55	1310e	0.40	2110e	0.05
2876.5871f	(5,1,2)	0510f	0.55	1310f	0.40	2110f	0.05
3020.9053e	(5,1,3)	2110e	0.39	0510e	0.37	1310e	0.24
3020.9083f	(5,1,3)	2110f	0.39	0510f	0.37	1310f	0.24
3050.5796f	(5,3,5)	1330f	0.67	0530f	0.32		
3050.5796e	(5,3,5)	1330e	0.67	0530e	0.32		
3136.3864e	(5,1,4)	2110e	0.56	1310e	0.36	0510e	0.08
3136.3885f	(5,1,4)	2110f	0.56	1310f	0.36	0510f	0.08
3333.7390e	(6,0,1)	0201e	0.87	1001e	0.13		
3346.5367f	(6,2,1)	0221f	1.00				
3346.5367e	(6,2,2)	0221e	1.00				
3439.3697e	(6,0,2)	1400e	0.45	0600e	0.43	2200e	0.11
3443.6498e	(6,0,3)	1001e	0.86	0201e	0.13		
3450.4696f	(6,2,2)	0620f	0.48	1420f	0.44	2220f	0.08
3450.4696e	(6,2,5)	0620e	0.48	1420e	0.44	2220e	0.08
3589.9285e	(6,0,4)	2200e	0.44	0600e	0.41	3000e	0.08
3604.4652f	(6,2,3)	2220f	0.44	0620f	0.41	1420f	0.15
3604.4652e	(6,2,7)	2220e	0.44	0620e	0.41	1420e	0.15
3712.1288e	(6,0,5)	3000e	0.43	1400e	0.34	0600e	0.14
3736.2254e	(6,2,9)	2220e	0.47	1420e	0.41	0620e	0.11
3736.2254f	(6,2,4)	2220f	0.47	1420f	0.41	0620f	0.11
3795.4517e	(6,0,6)	3000e	0.48	2200e	0.35	1400e	0.14
3897.5795e	(7,1,1)	0311e	0.78	1111e	0.21		
3897.5822f	(7,1,1)	0311f	0.78	1111f	0.21		
3920.6800e	(7,3,2)	0331e	1.00				
3920.6800f	(7,3,2)	0331f	1.00				
4023.0899e	(7,1,3)	1111e	0.78	0311e	0.21		
4023.0916f	(7,1,3)	1111f	0.78	0311f	0.21		
4163.5028e	(7,1,4)	2310e	0.42	0710e	0.42	3110e	0.15
4163.5071f	(7,1,4)	2310f	0.42	0710f	0.42	3110f	0.15
4297.5228e	(7,1,5)	3110e	0.48	1510e	0.31	0710e	0.19
4297.5261f	(7,1,5)	3110f	0.48	1510f	0.31	0710f	0.19
4373.6058e	(8,0,1)	0002e	0.99				
4405.6412e	(7,1,6)	2310e	0.40	3110e	0.35	1510e	0.20
4405.6438f	(7,1,6)	2310f	0.40	3110f	0.35	1510f	0.20
4452.1172e	(8,0,2)	0401e	0.64	1201e	0.33	2001e	0.02
4463.6263f	(8,2,1)	0421f	0.72	1221f	0.27		
4463.6263e	(8,2,3)	0421e	0.72	1221e	0.27		
4495.9161f	(8,4,2)	0441f	1.00				
4495.9161e	(8,4,4)	0441e	1.00				
4585.6695e	(8,0,4)	1201e	0.41	0401e	0.31	2001e	0.27
4602.4580e	(8,2,7)	1221e	0.72	0421e	0.27		
4602.4580f	(8,2,3)	1221f	0.72	0421f	0.27		
4679.9192e	(8,0,5)	2001e	0.68	1201e	0.25		
4726.8430e	(8,0,6)	0800e	0.40	2400e	0.32	3200e	0.25
4739.8194f	(8,2,4)	0800f	0.40	2400f	0.32	3200f	0.25
4739.8194e	(8,2,10)	0820e	0.42	2420e	0.37	3220e	0.20

Table 7 (continued)

<i>E</i> (cm ⁻¹)	GA ^a	SA ^b	F ^c	SA ^b	F ^c	SA ^b	F ^c
4866.8915e	(8,0,7)	3200e	0.36	0800e	0.24	1600e	0.21
4885.2212f	(8,2,5)	3220f	0.48	1620f	0.28	0820f	0.23
4885.2212e	(8,2,12)	3220e	0.48	1620e	0.28	0820e	0.23
4931.3147e	(9,1,1)	0112e	0.99				
4931.3161f	(9,1,1)	0112f	0.99				
4976.6505e	(8,0,8)	4000e	0.53	1600e	0.22	2400e	0.17
5010.3549e	(9,1,2)	0511e	0.55	1311e	0.40	2111e	0.05
5010.3589f	(9,1,2)	0511f	0.55	1311f	0.40	2111f	0.05
5011.5734e	(8,2,14)	2420e	0.41	3220e	0.28	1620e	0.25
5031.5519e	(9,1,3)	0531e	0.68	1331e	0.32		
5054.9088e	(8,0,9)	3200e	0.34	4000e	0.27	2400e	0.25
5153.3313e	(9,1,4)	2111e	0.38	0511e	0.37	1311e	0.24
5153.3343f	(9,1,4)	2111f	0.38	0511f	0.37	1311f	0.24
5267.5129e	(9,1,5)	2111e	0.55	1311e	0.35	0511e	0.08
5267.5150f	(9,1,5)	2111f	0.55	1311f	0.35	0511f	0.08
5294.4717e	(9,1,6)	0910e	0.38	3310e	0.31	2510e	0.22
5294.4772f	(9,1,6)	0910f	0.38	3310f	0.31	2510f	0.22
5442.5524e	(9,1,7)	0910e	0.28	4110e	0.26	3310e	0.24
5442.5570f	(9,1,7)	0910f	0.28	4110f	0.26	3310f	0.24
5477.9189e	(10,0,1)	0202e	0.86	1002e	0.13		
5490.2503e	(10,2,2)	0222e	0.99				
5490.2503f	(10,2,1)	0222f	0.99				
5567.3339e	(9,1,8)	4110e	0.48	1710e	0.26	0910e	0.11
5567.3375f	(9,1,8)	4110f	0.48	1710f	0.26	0910f	0.11
5587.8617e	(10,0,3)	1002e	0.85	0202e	0.13	3001e	0.02
5672.4713e	(9,1,9)	3310e	0.34	2510e	0.30	4110e	0.19
5672.4747f	(9,1,9)	3310f	0.34	2510f	0.30	4110f	0.19
5709.2500e	(10,0,5)	2201e	0.44	0601e	0.40	1401e	0.07
5723.3131e	(10,2,9)	2221e	0.43	0621e	0.41	1421e	0.15
5723.3131f	(10,2,4)	2221f	0.43	0621f	0.41	1421f	0.15
5829.9090e	(10,0,6)	3001e	0.40	1401e	0.33	0601e	0.13
5853.3109e	(10,2,11)	2221e	0.47	1421e	0.40	0621e	0.11
5853.3109f	(10,2,5)	2221f	0.47	1421f	0.40	0621f	0.11
5911.9476e	(10,0,8)	3001e	0.46	2201e	0.33	1401e	0.14
6005.8556e	(10,0,9)	4200e	0.34	0a00e	0.30	2600e	0.17
6021.3741e	(10,2,16)	4220e	0.32	0a20e	0.30	3420e	0.15
6021.3741f	(10,2,7)	4220f	0.32	0a20f	0.30	3420f	0.15
6028.1371e	(11,1,1)	0312e	0.78	1112e	0.21		
6028.1397f	(11,1,1)	0312f	0.78	1112f	0.21		
6050.3951e	(11,3,2)	0332e	0.99				
6050.3951f	(11,3,2)	0332f	0.99				
6135.3657e	(10,0,10)	5000e	0.28	1800e	0.21	4200e	0.17
6153.2007e	(11,1,3)	1112e	0.77	0312e	0.21	3111e	0.02
6153.2024f	(11,1,3)	1112f	0.77	0312f	0.21	3111f	0.02
6159.5781f	(10,2,8)	4220f	0.43	1820f	0.27	0a20f	0.14
6159.5781e	(10,2,18)	4220e	0.43	1820e	0.27	0a20e	0.14
6232.9149e	(10,0,11)	5000e	0.51	1800e	0.15	2600e	0.15
6269.6724e	(11,1,5)	0711e	0.42	2311e	0.41	3111e	0.14
6269.6766f	(11,1,5)	0711f	0.42	2311f	0.41	3111f	0.14
6283.6800f	(10,2,9)	2620f	0.32	3420f	0.32	1820f	0.17
6283.6800e	(10,2,20)	2620e	0.32	3420e	0.32	1820e	0.17
6315.0126e	(10,0,12)	3400e	0.30	4200e	0.24	2600e	0.22
6401.6560e	(11,1,6)	3111e	0.46	1511e	0.31	0711e	0.18
6401.6592f	(11,1,6)	3111f	0.46	1511f	0.31	0711f	0.18
6507.9053e	(11,1,8)	2311e	0.38	3111e	0.33	1511e	0.20
6507.9078f	(11,1,8)	2311f	0.38	3111f	0.33	1511f	0.20
6515.9860e	(12,0,1)	0003e	0.98	2002e	0.02		
6569.5469e	(12,0,2)	0402e	0.65	1202e	0.32	2002e	0.02
6574.4432e	(11,1,9)	4310e	0.33	0b10e	0.31	2710e	0.21
6702.3493e	(12,0,4)	1202e	0.41	0402e	0.30	2002e	0.26
6713.4260e	(11,1,10)	5110e	0.36	3510e	0.21	0b10e	0.18
6713.4309f	(11,1,10)	5110f	0.36	3510f	0.21	0b10f	0.18
6718.6083f	(12,2,3)	1222f	0.71	0422f	0.27	3221f	0.01
6718.6083e	(12,2,7)	1222e	0.71	0422e	0.27	3221e	0.01
6795.9320e	(12,0,6)	2002e	0.66	1202e	0.25	0402e	0.04
6830.7417e	(11,1,11)	5110e	0.38	1910e	0.20	4310e	0.18
6830.7457f	(11,1,11)	5110f	0.38	1910f	0.20	4310f	0.18
6937.6713e	(11,1,12)	3510e	0.30	2710e	0.24	4310e	0.22
6937.6755f	(11,1,12)	3510f	0.30	2710f	0.24	4310f	0.22
6957.9051e	(12,0,8)	3201e	0.35	0801e	0.23	1601e	0.20

Table 7 (continued)

E (cm $^{-1}$)	GA ^a	SA ^b	F ^c	SA ^b	F ^c	SA ^b	F ^c
6975.7480f	(12,2,6)	3221f	0.47	1621f	0.27	0821f	0.22
6975.7480e	(12,2,15)	3221e	0.47	1621e	0.27	0821e	0.22
7059.5368e	(13,1,1)	0113e	0.98	2112e	0.01		
7059.5382f	(13,1,1)	0113f	0.98	2112f	0.01		
7065.5225e	(12,0,10)	4001e	0.49	1601e	0.21	2401e	0.16
7099.8796e	(12,2,18)	2421e	0.40	3221e	0.26	1621e	0.24
7142.1299e	(12,0,12)	3201e	0.32	2401e	0.25	4001e	0.24
7256.4925e	(13,1,4)	0512e	0.36	2112e	0.36	1312e	0.25
7369.5187e	(13,1,6)	2112e	0.53	1312e	0.35	0512e	0.07
7369.5207f	(13,1,6)	2112f	0.53	1312f	0.35	0512f	0.07
7394.2747e	(12,0,14)	6000e	0.41	4400e	0.19	1a00e	0.18
7482.8544e	(12,0,15)	6000e	0.36	5200e	0.24	2800e	0.14
7592.4861e	(14,0,1)	0203e	0.86	1003e	0.12	2202e	0.01
7604.4227f	(14,2,1)	0223f	0.99	2222f	0.01		
7604.4227e	(14,2,2)	0223e	0.99	2222e	0.01		
7642.5439e	(13,1,10)	4111e	0.44	1711e	0.25	0911e	0.11
7642.5474f	(13,1,10)	4111f	0.44	1711f	0.25	0911f	0.11
7702.5015e	(14,0,3)	1003e	0.84	0203e	0.12	3002e	0.04
7918.5956e	(14,0,7)	3002e	0.38	1402e	0.33	0602e	0.13
7999.4293e	(14,0,9)	3002e	0.43	2202e	0.32	1402e	0.13
8253.9064e	(15,1,3)	1113e	0.76	0313e	0.20	3112e	0.03
8253.9080f	(15,1,3)	1113e	0.76	0313e	0.20	3112e	0.03
8292.1272e	(14,0,14)	5001e	0.45	1801e	0.15	2601e	0.14
8628.6843e	(16,0,1)	0004e	0.97	2003e	0.03		
8882.4982e	(16,0,6)	2003e	0.61	1203e	0.25	4002e	0.07

^a GA is the generalized (cluster) assignment (P, ℓ_2, i).^b SA is the spectroscopic (HITRAN) assignment V_1, V_2, ℓ_2, V_3, C , characters a,b,c in the V_2 field correspond to $V_2=10$, $V_2=11$, and $V_2=12$.^c Squares of the expansion coefficients of the vibrational state for the dominant basis states appearing in the preceding column.

Table 8
Observed local perturbations of the vibration-rotation states of $^{15}\text{N}^{14}\text{N}^{16}\text{O}$.

State	Perturber	$J_{\text{pert}}^{\text{a}}$	Type of interaction
1001e (6,0,3)	1400e (6,0,2)	25	anharmonic
1111e (7,1,3)	1510e (7,1,2)	56	anharmonic
1111f (7,1,3)	1510f (7,1,2)	49	anharmonic
1201e (8,0,4)	1620e (8,2,5)	42	anharmonic+ ℓ -type
1201e (8,0,4)	1600e (8,0,3)	63	anharmonic
4110e (9,1,8)	1401e (10,0,2)	47	Coriolis
5110e (11,1,11)	0801e (12,0,7)	67	Coriolis
0312e (11,1,1)	4200e (10,0,9)	81	Coriolis
0003e (12,0,1)	2311e (11,1,8)	56	Coriolis

^a Value of the angular momentum quantum number at which the energy level crossing takes place.

Interactions between vibrational states 1001e, 0600e, and 1400e are due to anharmonic resonances. These intrapolyad resonance interactions are explicitly taken into account by our model of H^{eff} and we have not any difficulty to fit rotational structure of these states. All other types of local perturbations found are summarized in Table 8. For each perturbed state we give both approximate spectroscopic assignment and exact cluster assignment, the perturber, and J value at which the energy level crossing takes place. In all cases we attributed perturbations to anharmonic resonances but not to Coriolis ones as it was stated by Amiot. We confirm Amiot's conclusion about perturbations of the 1111f (7,1,3) state at $J=49$ and of the 1201e (8,0,4) state at $J=42$. The perturbers are 1510f (7,1,2) and 1620e

(8,2,5) dark vibrational states located at 4005.867 cm $^{-1}$ and at 4564.445 cm $^{-1}$, respectively. The 1201e (8,0,4) vibrational state is perturbed additionally at $J=63$ by the 1600e (8,0,3) state. We have found that the 1111e (7,1,2) vibrational state is also perturbed by the 1510e (7,1,2) state at $J=56$. All these intrapolyad resonance interactions are explicitly taken into account by our model.

Among the local perturbations presented in Table 8 there are perturbations caused by interpolyad resonance Coriolis interactions which are not taken into account by our polyad model of H^{eff} . This prevents a good reproduction of the line positions of the respective bands. In Fig. 3, as an example, we present the residuals between observed and calculated line positions for the 4110–0110 band. The upper substate 4110e (9,1,8) of this band is perturbed by the 1401e (10,0,2) state by means of interpolyad resonance Coriolis interaction (energy level crossing at $J=47$). We pay attention of the readers on the different behavior of the residuals for the 4110e–0110e and the 4110f–0110f subbands. Only perturbed subband 4110e–0110e shows the resonance behavior of the residuals.

In addition to the local resonance Coriolis perturbations we have found two cases of the smooth interpolyad resonance Coriolis interactions. The respective vibrational states have very close energies at low J values but they do not cross. In the first case the vibrational states 0621 (10,2,4) and 4110 (9,1,8) perturb each other. The energy difference between levels in this case is about 2.1 cm $^{-1}$ for $J=2$. The vibrational states 2420 (8,2,14) and 0511 (9,1,2) are also in interpolyad resonance Coriolis interaction. The energy difference between levels at $J=2$ is

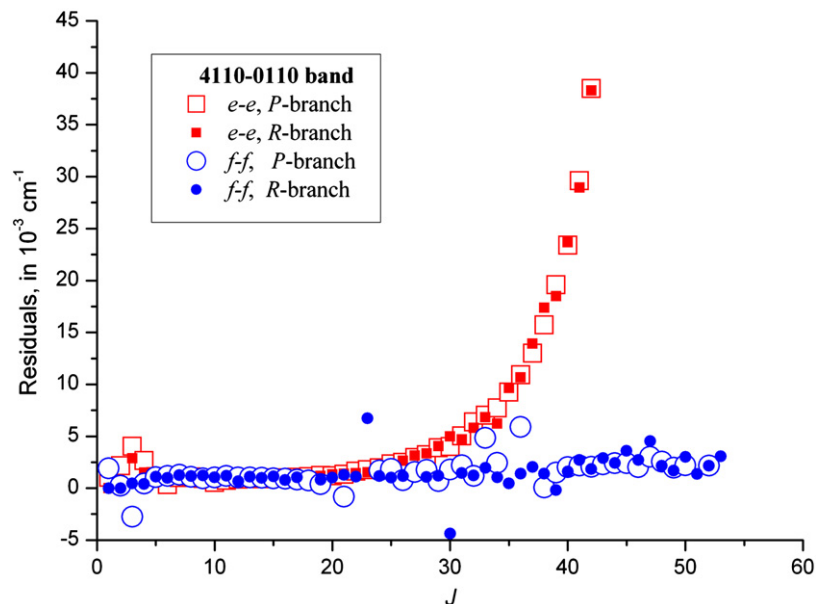


Fig. 3. The residuals between observed and calculated line positions of the 4110-0110 band. The upper vibrational state 4110e (9,1,8) of the 4110e-0110e subband is perturbed by the 1401e (10,0,2) vibrational state by means of an interpolyad resonance Coriolis interaction. For each J' value, the residuals were obtained from $P(J'+1)$ transitions and $R(J'-1)$ transitions.

Table 9

Summary of HITRAN-2008 $^{14}\text{N}^{15}\text{N}^{16}\text{O}$ and $^{15}\text{N}^{14}\text{N}^{16}\text{O}$ data.

Isotopologue	Lines	Frequency range (cm^{-1})	Intensity range (cm/molecule)	$ierr=0$	$ierr=4$
$^{14}\text{N}^{15}\text{N}^{16}\text{O}$	4222	5.0–5085.7	5.22×10^{-26} – 3.42×10^{-21}	49	4173
$^{15}\text{N}^{14}\text{N}^{16}\text{O}$	4592	4.9–4703.0	4.72×10^{-26} – 3.51×10^{-21}	51	4541

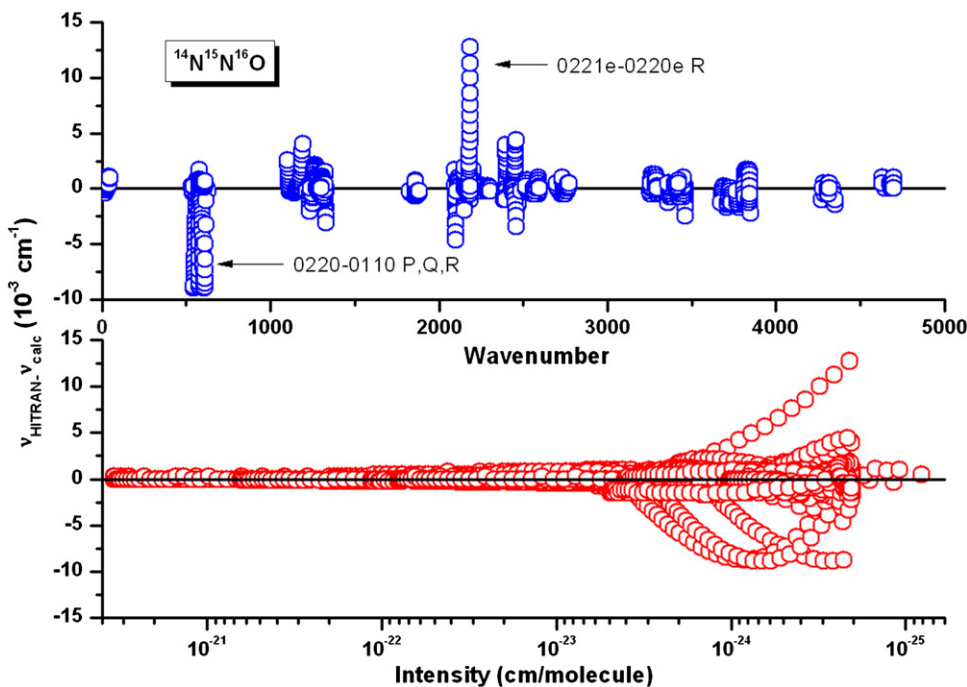


Fig. 4. Comparison of HITRAN-2008 and calculated line positions for $^{14}\text{N}^{15}\text{N}^{16}\text{O}$.

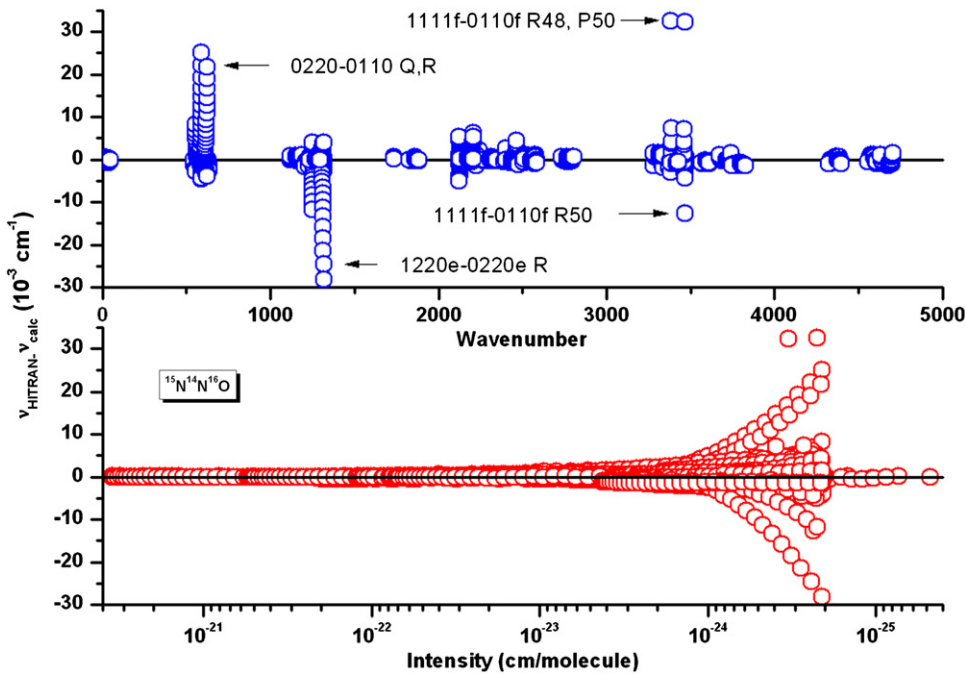


Fig. 5. Comparison of HITRAN-2008 and calculated line positions for $^{15}\text{N}^{14}\text{N}^{16}\text{O}$.

0.39 cm^{-1} for e sublevel and 0.41 cm^{-1} for f sublevel. For the bands involving these four interacting vibrational states we have rather large residuals reaching 0.01 cm^{-1} and even larger for some lines.

8. Comparison with HITRAN

HITRAN-2008 data [7] for $^{14}\text{N}^{15}\text{N}^{16}\text{O}$ and $^{15}\text{N}^{14}\text{N}^{16}\text{O}$ are summarized in Table 9. Isotopologue identifier is given in column 1. Column 2 contains the number of lines. Frequency and intensity ranges are given in columns 3 and 4, respectively. Finally in columns 5 and 6 are given the number of lines having 0 and 4 as position uncertainty indices. The most part of data are from Toth's calculated linelists [19] and have *ierr*=4 as position uncertainty index. This means that the estimated accuracy of these data lies between 0.0001 and 0.001 cm^{-1} . The linelists have been generated from spectroscopic constants given in previous studies of this author. A few of microwave data were taken from a previous version of HITRAN [33]. It is interesting to compare HITRAN-2008 line positions with positions which were calculated using fitted H^{eff} model obtained in this study.

For $^{14}\text{N}^{15}\text{N}^{16}\text{O}$ this comparison is summarized in Fig. 4. The upper panel shows the plot of the residual $\nu_{\text{HITRAN}} - \nu_{\text{calc}}$ versus wavenumber. The plot of the residuals versus line intensity is shown in the lower panel. It is seen that residuals of the most part of data lie within $\pm 0.001 \text{cm}^{-1}$. However, there are several branches which have rather big residuals (reaching 0.015 cm^{-1}) for large values of *J*. In all cases the transitions originate from the 0220 vibrational state. The lower panel of Fig. 4 shows that these lines are rather weak.

The similar comparison for $^{15}\text{N}^{14}\text{N}^{16}\text{O}$ is given in Fig. 5. Again, the residuals of the most part of the data lie within $\pm 0.001 \text{cm}^{-1}$ and abnormally large residuals (reaching 0.035 cm^{-1}) are found for the lines originating from the 0220 vibrational state. The lower panel of Fig. 5 shows that these lines are also rather weak.

9. Conclusion

The present work demonstrates that the polyad model of H^{eff} works well for the overwhelming majority of the observed bands of $^{14}\text{N}^{15}\text{N}^{16}\text{O}$ and $^{15}\text{N}^{14}\text{N}^{16}\text{O}$. The quality of modeling in general is compatible with uncertainties of the measurements. But as in the case of the principal isotopologue $^{14}\text{N}_2^{16}\text{O}$, there are few bands which are perturbed by interpolyad resonance Coriolis interactions. In the energy region below 8000 cm^{-1} which was involved in this study we did not meet any interpolyad resonance anharmonic interactions. In spite of the appearance of interpolyad resonance Coriolis interactions we believe that extrapolation properties of the fitted models are sufficient to help experimentalists to search and assign new bands of these isotopologues.

Acknowledgments

This work is jointly supported by NSFC-China (Grant nos. 20903085 and 10574124) and RFBR-Russia (Grant no. 06-05-39016). SAT and RVK thank also support from a joint RFBR-Russia (Grant no. 09-05-92508) and CRDF-USA (Grant no. RUG-2954-T0-09) Grant.

References

- [1] Campargue A, Weirauch G, Tashkun SA, Perevalov VI, Teffo JL. Overtone spectroscopy of N₂O between 10 000 and 12 000 cm⁻¹: a test of the polyad approach. *J Mol Spectrosc* 2001;209:198–206.
- [2] Vlasova AV, Perevalov BV, Tashkun SA, Perevalov VI. Global fittings of the line positions of the rare isotopic species of the nitrous oxide molecule. In: Proceedings of the XVth symposium on high-resolution molecular spectroscopy, Nizhny Novgorod, Russia. SPIE 2006; 6580:658007.
- [3] Ni HY, Song KF, Perevalov VI, Tashkun SA, Liu AW, Wang L, et al. Fourier-transform spectroscopy of ¹⁴N¹⁵N¹⁶O in the 3800–9000 cm⁻¹ region and global modeling of its absorption spectrum. *J Mol Spectrosc* 2008;248:41–60.
- [4] Song KF, Liu AW, Ni HY, Hu SM. Fourier-transform spectroscopy of ¹⁵N¹⁴N¹⁶O in the 3500–9000 cm⁻¹ region. *J Mol Spectrosc* 2009;255:24–31.
- [5] Lyulin OM, Jacquemart D, Lacome N, Tashkun SA, Perevalov VI. Line parameters of ¹⁵N₂¹⁶O from Fourier transform measurements in 5000–10 000 cm⁻¹ and global fitting of the line positions. *JQSRT* 2010;111:345–56.
- [6] Wang CY, Liu AW, Perevalov VI, Tashkun SA, Song KF, Hu SM. High-resolution infrared spectroscopy of ¹⁴N¹⁵N¹⁶O and ¹⁵N¹⁴N¹⁶O in the 1200–3500 cm⁻¹ region. *J Mol Spectrosc* 2009;257:94–104.
- [7] Rothman LS, Gordon IE, Barbe A, Benner DC, Bernath PF, Birk M, et al. The HITRAN 2008 molecular spectroscopic database. *JQSRT* 2009;110:553–72.
- [8] Teffo JL, Perevalov VI, Lyulin OM. Reduced effective Hamiltonian for a global treatment of rovibrational energy levels of nitrous oxide. *J Mol Spectrosc* 1994;168:390–403.
- [9] Teffo JL, Chedin A. Internuclear potential and equilibrium structure of the nitrous oxide molecule from rovibrational data. *J Mol Spectrosc* 1989;135:389–409.
- [10] Coles DK, Hudges RH. Microwave spectra of nitrous oxide. *Phys Rev* 1949;76:178.
- [11] Andreev BA, Burenin AB, Karyakin EN, Krupnov AF, Shapin SM. Submillimeter wave spectrum and molecular constants of N₂O. *J Mol Spectrosc* 1976;62:125–48.
- [12] Morino I, Fabian M, Takeo H, Yamada KMT. High-*J* rotational transitions of NNO measured with the NAIR terahertz spectrometer. *J Mol Spectrosc* 1997;185:142–6.
- [13] Drouin BJ, Maiwald FW. Extended THz measurements of nitrous oxide, N₂O. *J Mol Spectrosc* 2006;236:150–2.
- [14] Hinz A, Wells JS, Maki AG. Heterodyne measurements of hot bands and isotopic transitions of N₂O near 7.8 μm. *Z Phys D* 1987;5:351–8.
- [15] Brown LR, Toth RA. Comparison of the frequencies of NH₃, CO₂, H₂O, N₂O, CO and CH₄ as infrared calibration standards. *J Opt Soc Am* 1985;2:842–56.
- [16] Toth RA. Frequencies of N₂O in the 1100–1440-cm⁻¹ region. *J Opt Soc Am* 1986;3:1263–81.
- [17] Toth RA. N₂O vibration-rotation parameters derived from measurements in the 900–1090 and 1580–2380 cm⁻¹ regions. *J Opt Soc Am* 1987;4:357–74.
- [18] Toth RA. Line-frequency measurements and analysis of N₂O between 900 and 4700 cm⁻¹. *Appl Opt* 1991;30:5289–315.
- [19] Toth RA. Linelist of N₂O parameters from 500 to 7500 cm⁻¹. Available via WEB site www.mark4sun.jpl.nasa.gov.
- [20] Krell JM, Sams RL. Vibration-rotation bands of nitrous oxide: 4.1 micron region. *J Mol Spectrosc* 1974;51:492–507.
- [21] Amiot C. Vibration-rotation bands of ¹⁴N¹⁵N¹⁶O–¹⁵N¹⁴N¹⁶O 1.6–5.7 μm region. *J Mol Spectrosc* 1976;59:191–208.
- [22] Guelachvili G, Narahari Rao K. Handbook of infrared standards, with spectral maps and transition assignments between 3 and 2600 μm. Orlando Florida: Academic Press; 1986.
- [23] Wang L, Perevalov VI, Tashkun SA, Gao B, Hao LY, Hu SM. Fourier transform spectroscopy of N₂O weak overtone transitions in the 1–2 μm region. *J Mol Spectrosc* 2006;237:129–36.
- [24] Liu AW, Kassi S, Malara P, Romanini D, Perevalov VI, Tashkun SA, et al. High sensitivity CW-cavity ring down spectroscopy of N₂O near 1.5 μm (I). *J Mol Spectrosc* 2007;244:33–47.
- [25] Liu AW, Kassi S, Perevalov VI, Tashkun SA, Campargue A. High sensitivity CW-cavity ring down spectroscopy of N₂O near 1.5 μm (II). *J Mol Spectrosc* 2007;244:48–62.
- [26] Herbin H, Picqué N, Guelachvili G, Sorokin E, Sorokina IT. N₂O weak lines observed between 3900 and 4050 cm⁻¹ from long path absorption spectra. *J Mol Spectrosc* 2008;238:256–9.
- [27] Tashkun SA, Perevalov VI, Teffo JL, Lecoutre M, Huet TR, Campargue A, et al. ¹³C¹⁶O₂: Global treatment of vibrational-rotational spectra and first observation of the 2v₁+5v₃ and v₁+2v₂+5v₃ absorption bands. *J Mol Spectrosc* 2000;200:162–76.
- [28] Furtenbacher T, Császár AG, Tennyson J. MARVEL: measured active rotational-vibrational energy levels. *J Mol Spectrosc* 2007;245:115–25.
- [29] Guelachvili G, Birk M, Bordé CJ, Brault JW, Brown LR, Carli B, et al. High resolution wavenumber standards for the infrared. *J Mol Spectrosc* 1996;177:164–79.
- [30] Tashkun SA, Perevalov VI, Teffo JL, Rothman LS, Tyuterev VIG. Global fitting of ¹²C¹⁶O₂ vibrational-rotational line positions using the effective Hamiltonian approach. *JQSRT* 1998;60:785–801.
- [31] Bunch DS, Gay DM, Welsch RE. Algorithm 717: subroutines for maximum likelihood and quasi-likelihood estimation of parameters in nonlinear regression models. *ACM Trans Math Software* 1993;19:109–30.
- [32] Ni HY. Private communication, 2007.
- [33] Rothman LS, Gamache RR, Goldman A, Brown LR, Toth RA, Pickett HM, et al. The HITRAN database: 1986 edition. *Appl Opt* 1987;26:4058–97.